Biosensors and Bioelectronics 135 (2019) 216–223

Contents lists available at ScienceDirect

Biosensors and Bioelectronics

journal homepage: www.elsevier.com/locate/bios

Highly sensitive and wide-range nanoplasmonic detection of fibrinogen using erythrocyte membrane-blanketed nanoparticles

Seongjae Jo[a,1], Insu Kim[b,1], Wonseok Lee[a,1], Minwoo Kim[a], Joohyung Park[a], Gyudo Lee[b], Dae Sung Yoon[b,*], Jinsung Park[a,**]

[a] Department of Control and Instrumentation Engineering, Korea University, Sejong, 30019, South Korea
[b] School of Biomedical Engineering, Korea University, Seoul, 02841, South Korea

ARTICLE INFO

Keywords:
Erythrocyte membrane
Fibrinogen
Localized surface plasmon resonance
Gold nanoparticle
Human plasma

ABSTRACT

Fibrinogen, which is a glycoprotein that circulates in the blood, plays various important biological roles, *e.g.,* in blood coagulation, fibroblast proliferation, angiogenesis, and wound healing. Abnormal levels of fibrinogen in plasma have been identified as a key biomarker of a variety of disorders from cardiovascular diseases to hemophilia. Therefore, the development of a quantitative assay for fibrinogen in the blood has emerged as an important issue for the prevention and diagnosis of these diseases. Meanwhile, it is well known that erythrocytes can selectively capture fibrinogen because of the fibrinogen receptor expressed on their plasma membrane. Inspired by these biological interactions, herein, we devised an erythrocyte membrane (EM)-blanketed biosensor based on localized surface plasmon resonance (LSPR) for highly sensitive detection of fibrinogen. By placing the EM onto a nanoparticle-on-substrate, we enhanced the LSPR signal, achieving highly sensitive and selective detection of fibrinogen. We demonstrated that fibrinogen detection is possible over a wide concentration range, 0.001–5.000 mg/mL, which can cover normal and pathological blood fibrinogen levels. In addition, it was verified that the biosensor selectively detects fibrinogen in comparison with other human-blood-plasma components. The nanoplasmonic sensor blanketed with the EM opens up new opportunities for the development of a robust fibrinogen-sensing technology.

1. Introduction

Fibrinogen, which is produced by the liver, is a glycoprotein that circulates in the blood (Campuzano et al., 2014; Tennent et al., 2007). When a tissue or vascular injury occurs, fibrinogen is converted by thrombin to fibrin, to subsequently form blood clots (Wu et al., 1991). Through this process, fibrinogen blocks the damaged blood vessels and serves to stop excessive bleeding (Lowe et al., 2004; Levy et al., 2013). In addition, it has been reported that fibrinogen mediates many processes such as endothelial-cell spreading (Dejana et al., 1990), fibroblast proliferation (Sahni et al., 1999), capillary-tube formation (Bach et al., 1998), angiogenesis (Shiose et al., 2004), and wound healing (Laurens et al., 2006). The reference level of fibrinogen in human blood is 1.5–4.5 mg/mL (Chen et al., 2011; Lowe et al., 2004). Nonetheless, abnormal concentrations of fibrinogen in blood plasma can cause various disorders (Lowe et al., 2004). In particular, a lower concentration of fibrinogen increases the risk of bleeding because blood coagulation is inhibited; this condition is commonly known as hemophilia (Neerman-Arbez and Casini, 2018). Additionally, a higher concentration of fibrinogen has been identified as an important biomarker of cardiovascular disease (Ernst, 1993; Kaptoge et al., 2012). Recently, it was shown that in addition to its association with vascular diseases, fibrinogen is associated with cancer (Simpson-Haidaris and Rybarczyk, 2001). Fibrinogen is an important factor for the metastatic potential of circulating tumor cells (Palumbo et al., 2000) and has attracted much interest as a prognostic biomarker of survival of patients with ovarian (Polterauer et al., 2009) or gastric (Lee et al., 2004) cancer.

Due to the clinical importance of fibrinogen, the development of sensitive and selective assays for accurate detection of fibrinogen is still highly relevant in biomedical and clinical research. To date, many analytical methods for fibrinogen have been devised (Garvey and Black, 1972; Lowe et al., 2004). For example, the Clauss method is commonly used to detect fibrinogen via the measurement of clotting time in the presence of thrombin; this method has a detection range of

* Corresponding author.
** Corresponding author.
E-mail addresses: dsyoon@korea.ac.kr (D.S. Yoon), shinedew@korea.ac.kr (J. Park).
[1] These authors contributed equally to this work.

https://doi.org/10.1016/j.bios.2019.04.030
Received 31 January 2019; Received in revised form 20 March 2019; Accepted 15 April 2019
Available online 17 April 2019
0956-5663/

0.30–2.07 mg/mL (Miesbach et al., 2010). Similarly, the prothrombin time test has been developed, in which the fibrinogen concentration is estimated based on the process of clotting triggered by prothrombin; this method has a detection range of 0.97–4.87 mg/mL (Miesbach et al., 2010). Nevertheless, these assays have several problems: the results of these tests can differ depending on the analytical method and experimental conditions such as the blood sampling method, sample storage conditions, sample incubation time, and the incubation temperature (Mackie et al., 2003; Piccione et al., 2010).

Meanwhile, various immunological methods for fibrinogen sensing (*e.g.,* enzyme-linked immunosorbent assay [ELISA], radial immune diffusion, and immune nephelometric assay) have been reported (Brittin et al., 1972; Lowe et al., 2004; Schifreen et al., 1985). Electrochemical immune sensing and amperometric magnetoimmunosensing have been developed as improvements to this immunological assay (Campuzano et al., 2014). Nonetheless, these immunological assays require a label (*e.g.,* an antibody); thus, these methods for the detection of fibrinogen are costly. Recently, to overcome this obstacle, various nanoparticle-based assays have been developed (Chen et al., 2011). This method is based on fibrinogen–nanoparticle interactions for detection of fibrinogen without specific labeling. Despite these efforts, these nanoparticle-based detection methods can hardly cover the concentrations of fibrinogen associated with fibrinogen disorders caused by its excess or deficiency.

Among sensor methods, surface plasmon resonance (SPR) sensors have attracted attention due to efficient sensing capability. SPR is an optical phenomenon involving electromagnetic oscillations of free electrons propagating along the surface of a metal film through a prism (Yola et al. 2014a, 2014b). To date, SPR has been employed as a versatile detection method for analysis of various biomolecules through the measurement of changes in the refractive index (Atar et al., 2015a; Yola et al., 2015). Recently, techniques for coupling (of nanoparticles with thin metal films) and the molecular imprinting method involving a polymer were reported to enhance the SPR response in biosensors (Atar et al., 2015b; Özkan et al., 2019). Meanwhile, localized surface plasmon resonance (LSPR) of metal nanostructures—such as bulk solutions of nanoparticles, nanoparticle arrays, and single nanoparticles— is used to detect biomolecules through a shift of resonant wavelength in response to a refractive index change. LSPR-based sensors are crucial for the detection of biomolecules and biointeractions because this is a sensitive and label-free approach. Moreover, the LSPR method provides a convenient way to mass-produce and low-cost biosensors (Hong et al., 2018).

In this study, we developed a highly sensitive and selective nanoplasmonic biosensor of fibrinogen using erythrocyte membrane (EM)-blanketed gold nanoparticles (AuNPs). As the EMs are attached to the substrate, not only do the nanoparticles become well dispersed on the substrate, but the surface area of the substrate also increases, thereby improving the LSPR phenomenon and increasing sensitivity of the fibrinogen detection. The nanoparticles are well immobilized on the nanoplasmonic substrate and stay there even after various chemical treatments. In addition, this biosensor does not require additional labels such as antibodies and aptamers; EMs also increase the fibrinogen-capture efficiency of the sensor by taking advantage of the nature of the interaction between fibrinogen and its specific receptor present on the EM. Using this strategy, we demonstrated that highly sensitive fibrinogen detection by the nanoplasmonic sensor is possible over a wide concentration range, 0.001–5.000 mg/mL, in fibrinogen-spiked blood plasma samples. We believe that this detection strategy involving EMs has great potential for fibrinogen quantification and for the prevention of various fibrinogen-related disorders such as afibrinogenemia, cryofibrinogenemia, dysfibrinogenemia, hypofibrinogenemia, and even cardiovascular diseases.

2. Materials and methods

2.1. Materials and reagents

All chemical reagents, such as gold (III) chloride trihydrate ($HAuCl_4$), trisodium citrate, sulfuric acid (H_2SO_4), hydrogen peroxide (H_2O_2), 3-aminopropyltrimethoxysilane, fibrinogen from human plasma, human serum albumin (HSA), γ-globulin from human blood, and deionized (DI) water were purchased from Sigma-Aldrich, whereas phosphate-buffered saline (PBS, 1 × , pH 7.4, with calcium and magnesium) was from Gibco.

2.2. Extraction of EMs

Erythrocytes were isolated from whole human blood by a previously reported method (Kim et al., 2018). Whole blood was centrifuged at 1000 × *g* for 5 min at 4°C to separate erythrocytes from plasma and buffy coats. After that, the precipitate including erythrocytes was collected and washed thrice with 1 × PBS at 4°C, before hemolysis. The washed erythrocytes were resuspended in 0.25 × PBS for 20 min at 4°C for hemolysis. As a result, hemoglobin and membrane proteins were released into the solution. The hemolyzed suspension was centrifuged at 1000 × *g* for 5 min to separate the cytoplasmic components from the EM. The supernatant was removed, and the EM pellet was washed twice with 1 × PBS at 4°C.

2.3. Synthesis of AuNPs

Citrate-stabilized AuNPs were synthesized via the protocol reported by the Puntes group (Bastús et al., 2011). One hundred and fifty milliliters of a trisodium citrate solution (2.2 mM) was stirred by means of a magnetic bar at up to 100°C. After the temperature of the solution reached 100°C, 1 mL of an $HAuCl_4$ solution (25 mM) was added. The reagents were dispersed in DI water. The color of the solution changed to soft pink in 10 min. After this color change, the temperature of the solution was immediately reduced to 90°C. Then, 1 mL of the $HAuCl_4$ solution (25 mM) was injected into the reaction mixture. We added the same amount of the $HAuCl_4$ solution after 30 min. The reaction completed after 30 min. Finally, AuNPs were isolated from the resultant solution by centrifugation and were resuspended in DI water.

2.4. Fabrication of an AuNP-based LSPR biosensor and blanketing of the biosensor with EMs

The AuNP-based substrates for creation of the LSPR biosensor were fabricated by our method described in a previous work (Hong et al., 2018). The detailed process was as follows: A round cover slip (12 mm ∅), which was the substrate, was cleaned with the piranha solution (H_2SO_4 mixed with 30% H_2O_2 at 3:1). After that, the substrate was washed with DI water and dried. The substrate was functionalized with an amino group using 1 mL of an ethanol-based 4% 3-aminopropyltrimethoxysilane solution for 30 min to later immobilize the AuNPs on the substrate. After the reaction, the substrate was repeatedly rinsed with ethanol and DI water to ensure that the residual reagent was completely removed, and then the substrate was baked at 60°C for 2 h. Next, the amino group–functionalized coverslips were immersed in 1 mL of the AuNP solution for 1 h, to immobilize the AuNPs on the LSPR substrate, followed by washing with DI water. After the fabrication of the AuNP-based LSPR substrate, we created an EM-blanketed LSPR biosensor for high-sensitivity fibrinogen detection. To coat the AuNP-based LSPR substrate with the EMs, the substrate was immersed in 1 mL of a 0.05 v/v% EM suspension for 1 h. The substrate was then gently rinsed with DI water and dried.

2.5. Experimental setup and recording of LSPR spectra

The spectra of the fabricated substrates were recorded on our homemade LSPR sensing system. The sensing system and the LSPR spectrum acquisition process were as follows: white light from an HL-2000-FHSA tungsten-halogen light source (Ocean Optics) with a 2 mm beam diameter reached the substrate after passing through a collimating lens and a tilting mirror. The light penetrating through the substrate was analyzed by an HR4000 spectrometer (Ocean Optics). To improve the reproducibility and repeatability of the LSPR biosensor, we acquired the LSPR spectra at five points on three substrates.

2.6. Scanning electron microscopy (SEM) and atomic force microscopy (AFM) analyses of the LSPR biosensor

SEM images were captured by a Quanta 250 FEG field emission scanning electron microscope (Thermo Fisher Scientific). The LSPR biosensor was coated with platinum of thickness up to 1 nm. Additionally, to demonstrate the coating of the LSPR biosensor with EMs, we performed AFM under a scanning probe microscope (SPM-9700, Shimadzu, Japan) in tapping mode. The scan size of all images was 0.09 μm^2, and the scan rate was 0.6 Hz. The height analysis of the AFM images was performed in the SPM-9700 Analysis software (SPM-9700 Analysis, Shimadzu, Japan).

2.7. Fourier-transform infrared (FT-IR) spectroscopy

To cross-check the successful immobilization of EMs on the LSPR biosensor, we collected FT-IR spectra of the surface of the LSPR biosensor at a resolution of 4 cm^{-1} on a Spectrum 100 FT-IR spectrometer (PerkinElmer, USA). The spectrum of each sample was recorded in the range of 500–4000 cm^{-1}.

3. Results and discussion

3.1. Strategy of fibrinogen detection with the EM-blanketed LSPR biosensor

The fundamentals of configuration of the EM-blanketed AuNP–based LSPR biosensor for fibrinogen detection developed in this work are described in Fig. 1. We fabricated the nanoplasmonic substrate using AuNPs for fibrinogen detection via the LSPR system. First, we treated the clean glass substrate with a 3-aminopropyltrimethoxysilane solution for 30 min to later immobilize the AuNPs on the substrate. Then, the amino group–functionalized substrate was immersed in the AuNP solution for 1 h. We synthesized the AuNPs by a previously published protocol (Bastús et al., 2011) with some modifications. The absorbance spectra of the AuNPs, which were dispersed in solution, were acquired on an ultraviolet–visible spectrometer (Fig. S1). After the immobilization of the AuNPs, the substrate was analyzed by means of our homemade LSPR sensing system; we then confirmed that the LSPR phenomenon takes place on the fabricated substrate (dark grey line). As a result, we observed that the absorbance peak of the nanoplasmonic substrates was 507.88 ± 0.19 nm.

To effectively detect fibrinogen, we tested a strategy involving the coating of the AuNP-based LSPR substrate with EMs. The reasons for the use of EMs for effective sensing of fibrinogen are as follows. Recently, Guedes et al. reported that increased aggregation of erythrocytes is linked to high fibrinogen concentration in plasma (Guedes et al., 2017). This effect is related to the interaction between fibrinogen and integrin receptors on the EM (Carvalho et al. 2010, 2011; Guedes et al., 2017). From these results, we concluded that EMs can serve as a good material for capturing fibrinogen, and we utilized the strategy for increasing the fibrinogen sensing efficiency by blanketing the LSPR substrate with EMs. The AuNPs dispersed on the substrate were well immobilized by the EMs, thus overcoming such problems as the detachment and aggregation of AuNPs owing to washing or external influences on the substrate. In addition, the surface area of the LSPR substrate increased due to the nanoparticles, as compared to that when only EMs were present on the LSPR substrate. Moreover, the LSPR phenomenon on the substrate can be improved after EMs attach to the AuNP-based LSPR substrate (Fig. S2). These advantages improve LSPR of the substrate for fibrinogen detection. Therefore, this strategy can maximize the fibrinogen detection ability of LSPR.

To coat the AuNP-based LSPR substrate with EMs, the substrate was immersed in and reacted with the EM suspension for 1 h. After the EM-coating process, the EM-blanketed LSPR biosensor was ready. Using this LSPR system, we observed a red shift in the absorbance peak of the EM-blanketed LSPR biosensor (blue line). We then treated the biosensor with fibrinogen and found that the absorbance peak shifted remarkably (red line). Following this strategy, we presented the results of fibrinogen detection by the EM-blanketed LSPR biosensor, which was found to effectively detect fibrinogen, a major biomarker of various diseases.

3.2. Optimization of the AuNP-based LSPR substrate depending on binding time of AuNPs

The nanoplasmonic substrate is the most important component of a biosensor based on LSPR (Feuz et al., 2010). When the LSPR substrate is fabricated, the binding time of AuNPs is important because it can determine the amount of AuNPs deposited on the substrate or the distance between AuNPs. To optimize the nanoplasmonic substrate, we fabricated the LSPR substrate at different binding periods of AuNPs. We examined the LSPR spectra of the fabricated substrates while changing the binding time of the AuNPs on the substrate from 30 min to 2 h. As shown in Fig. 2a, the color of the LSPR substrate changed from light red to dark blue as a function of the binding time of AuNPs on the substrate. As depicted in Fig. 2b–d, we investigated the LSPR spectra of each substrate at different binding periods. As a result, we found that the absorption peak was weak at the AuNP-binding time of 30 min (Fig. 2b). This means that the AuNP-binding time of 30 min is not enough for the attachment of a sufficient amount of the AuNPs to the substrate, thereby reducing LSPR. On the contrary, at the binding time of 1 h, it was found that the intensity of the absorption peak was the highest (Fig. 2c). This finding indicates that many AuNPs were stably attached to the substrate in the 1-h binding condition. By contrast, when the binding time of the AuNPs on the substrate was longer than 2 h, another absorption peak emerged between 600 and 700 nm owing to aggregation of the particles (Figs. 2d and S3). This phenomenon coincided with the change of the substrate color from red to blue at the AuNP-binding time of 2 h (Fig. 2a). In addition, by SEM imaging, we confirmed that the AuNPs on the substrate were uniformly dispersed without particle aggregation at the binding time of 1 h (Fig. 2e). The size of the AuNPs was uniform: 20 nm (Fig. 2f). On the basis of the LSPR spectral results, we determined the optimum binding time of the AuNPs on the substrate to be 1 h.

3.3. Coating of the AuNP-based LSPR substrate with EMs

As mentioned above, we used a strategy of blanketing the AuNP-based LSPR substrate with the EM for effective fibrinogen detection. To verify whether the EMs were properly attached to the substrate, we performed AFM topology imaging (Fig. 3a). According to the topological AFM images of the AuNP-based LSPR substrate (*i.e.,* not blanketed with EMs) and EM-blanketed LSPR substrates, the height of the substrates was 20.09 ± 0.82 and 22.03 ± 1.06 nm, respectively. It was shown that the entire height of the AuNP-based LSPR substrate increased slightly after the EM blanketing, suggesting that the substrate was thoroughly coated with the EMs. Of note, after the SEM analysis, we found that the AuNPs were uniformly dispersed on the substrate after the blanketing of the AuNP-based LSPR substrate with the EMs (Fig. S4). After that, it was confirmed that the dispersion of AuNPs was

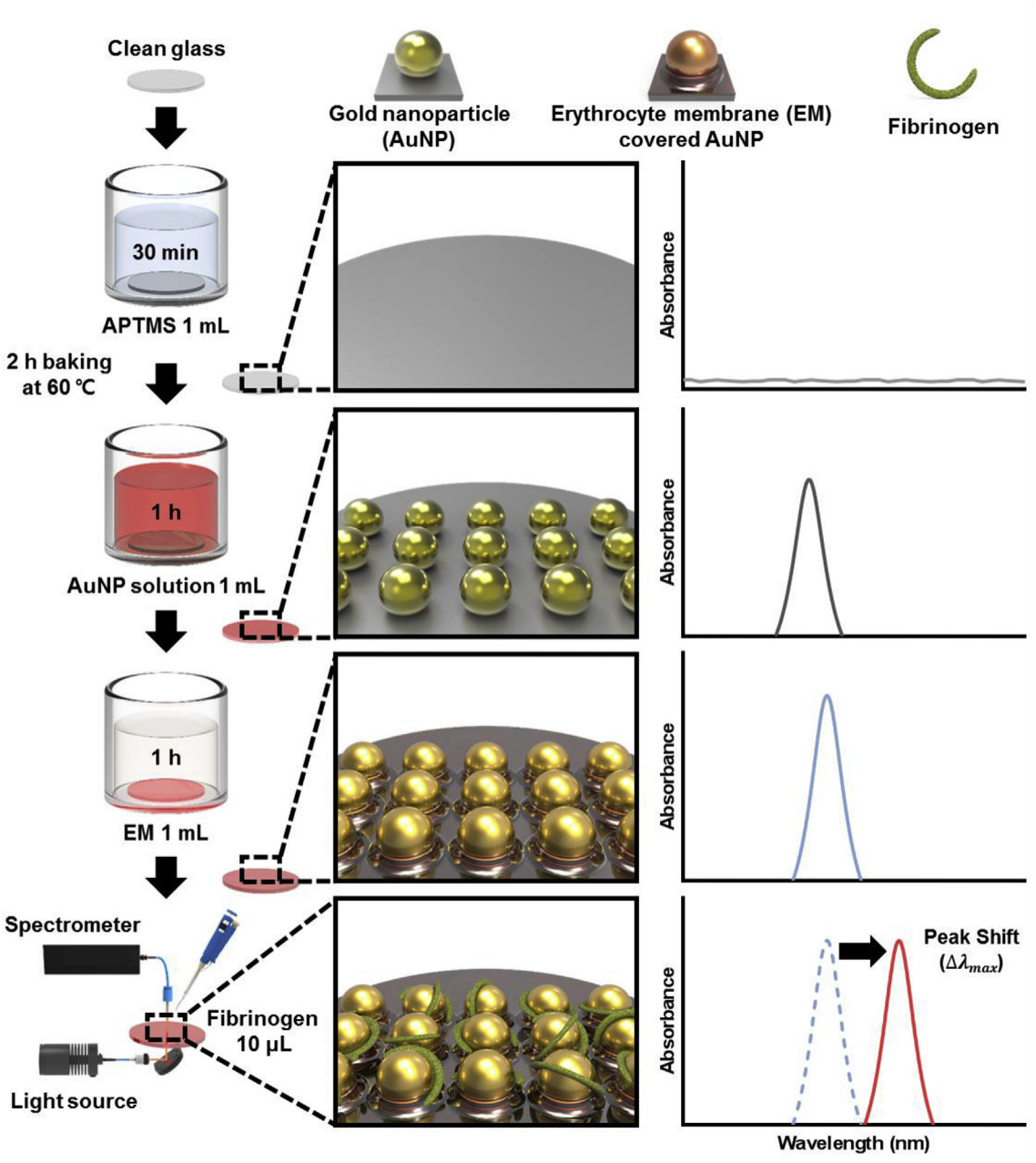

Fig. 1. Schematic diagram of proof-of-concept detection of fibrinogen using the EM-blanketed LSPR biosensor.

maintained after chemical treatment of the substrate, including washing with DI water; thus, the LSPR signal was stably detectable. To cross-check whether the EMs were attached well to the substrate, we performed FT-IR analysis. Novel FT-IR peaks were observed for the EM-blanketed LSPR biosensor, compared to the nonblanketed LSPR substrate (Fig. 3b). In particular, the FT-IR spectrum of the EM-blanketed LSPR substrate shows amide I, amide II, COO^- from carboxylate groups of proteins, and CH_2/CH_3 deformations from the lipids of the EM (Kozicki et al., 2015). Vibrations in the 3500–3100 cm^{-1} region derived from water O–H antisymmetric and symmetric stretching vibrations were observed too (Kozicki et al., 2015). In addition, we investigated the differences between the nonblanketed and EM-blanketed LSPR substrates by means of the LSPR system (Fig. 3c). Before the EM blanketing, the absorbance peak of the LSPR substrate was observed at 507.88 ± 0.19 nm. The absorbance peak of the LSPR substrate shifted to 514.01 ± 0.10 nm after the EM blanketing. Due to these differences, we confirmed that the LSPR phenomenon could be enhanced by the blanketing of the AuNP-based LSPR substrate with EMs.

Furthermore, reliability and reproducibility are key parameters that must be considered during biosensor design. Accordingly, many researchers have attempted to improve these parameters by chemical treatment of the sensor surface in a variety of ways (Grimaldi et al., 2016). By blanketing the substrate with EMs, we were able to uniformly distribute the fibrinogen receptor on the LSPR substrate. To demonstrate the reliability of the EM-blanketed LSPR biosensor and reproducibility of its results, we recorded LSPR spectra at several points on one LSPR substrate after treatment with fibrinogen (Fig. 3d). When the EMs were not present on the substrate, although the LSPR signal was detected, the LSPR spectra were uneven: varied among different regions. On the other hand, the LSPR spectra of the EM-blanketed LSPR biosensor were uniform in all the different regions. The consistency of the LSPR spectral results can be attributed to the fact that the fibrinogen receptors present on the EMs uniformly coat the LSPR substrate. These results indicate that fibrinogen can be detected in all LSPR substrate

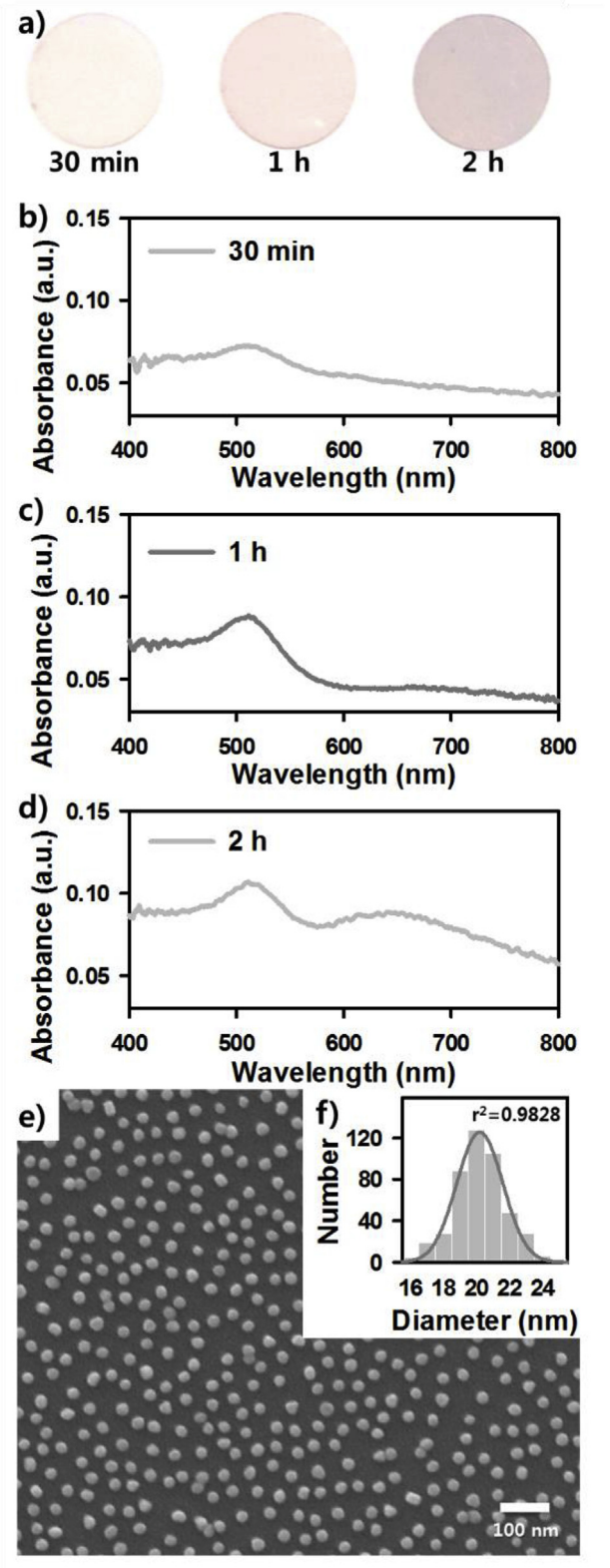

Fig. 2. LSPR effect depending on the binding time of AuNPs on the substrate. a) Optical images of the LSPR substrate after it was subjected to different AuNP-binding periods (30 min, 1 h, and 2 h). LSPR spectra of each substrate at the different AuNP-binding periods, b) 30 min, c) 1 h, and d) 2 h (a.u.: arbitrary units). e) SEM image of the LSPR substrate after the 1-h binding. f) Histogram of the particle size of the LSPR substrate after the 1-h binding.

regions because of the EMs, meaning that sensitivity of the LSPR sensor and reproducibility and repeatability of its results were increased by the EMs.

3.4. Analytical performance of the EM-blanketed LSPR sensor on fibrinogen detection

After coating the AuNP-based LSPR substrate with the EMs, we performed fibrinogen detection over a wide concentration range, 0.001–5.000 mg/mL, which covers both the normal and pathological blood fibrinogen levels (Fig. 4). Of note, in the SEM images, we found that EM-blanketed nanoparticles were wrapped in fibrinogen (Fig. 4a). This phenomenon is consistent with the results of studies by the Minchin group on the interaction between nanoparticles and fibrinogen (Deng et al., 2012). In particular, they reported that multiple protein molecules (*i.e.,* fibrinogen) can bind nanoparticles, thus leading to a highly packed fibrinogen corona, when the size of the nanoparticles is greater than 12 nm (Deng et al., 2012). In our experiments, the size of AuNPs was 20 nm, which means that fibrinogen can be packed among the particles and form a fibrinogen corona. The formation of the fibrinogen corona can lead to a red shift of the LSPR absorbance peak.

Meanwhile, to examine how the concentration of EMs on the LSPR substrate affects the fibrinogen sensing, we treated the substrate with a fixed concentration (0.01 mg/mL) of fibrinogen, while changing the concentration of the EMs (0.05–5.00 v/v%) on the substrate. First, before the fibrinogen treatment, we measured the absorbance of the LSPR substrate blanketed with different concentrations of EMs (Fig. S5). Next, we measured absorbance of the LSPR substrate after fibrinogen treatment (Fig. 4b). When the concentration of EMs was 5 v/v%, the shift in the LSPR absorbance peak ($\Delta\lambda_{max}$) of the substrate under the influence of fibrinogen treatment was almost negligible. Consequently, it is fair to say that when the LSPR substrate is covered with too much membrane, the red shift in the LSPR absorption peak due to fibrinogen decreases. The red shift is reduced because the EM-blanketed LSPR biosensor deviates from the measurable refractive index ranges. The absorbance peak shifted more at a low concentration of EMs (*i.e.,* 0.5 v/v%) than at their high concentration (*i.e.,* 5 v/v%), but this arrangement was still insufficient to effectively detect fibrinogen. When 0.05 v/v% EM was applied to the substrate, it was observed that the shift in the LSPR absorbance peak was significant after the fibrinogen reaction, as compared to that in the other EM-blanketing conditions. Accordingly, we found that there is an optimal EM-covering concentration for detection of the LSPR phenomenon after the reaction of the substrate with fibrinogen; the fibrinogen detection experiment was performed by fixing the EM concentration at 0.05 v/v%.

After optimization of the EM concentration on the LSPR substrate, we carried out a proof-of-concept experiment for fibrinogen detection over a wide concentration range, 0.001–5.000 mg/mL, in PBS. Our proof-of-concept detection of fibrinogen was successful (Fig. 4c); when the target protein (*i.e.,* fibrinogen in our experiment) was adsorbed on the surface of the LSPR biosensor, this adsorption induced a change in the refractive index of the LSPR substrate, which was monitored by means of the shift in the absorbance peak in the LSPR spectrum. In a control experiment, in the absence of fibrinogen treatment, the shift in the maximum absorbance peak ($\Delta\lambda_{max}$) was ~3 nm (black dashed line in Fig. 4c). This result may reflect a change in the refractive index owing to the presence of various ions in PBS. Due to the binding of fibrinogen to the LSPR substrate, $\Delta\lambda_{max}$ increased from 5 to 26 nm as the concentration of fibrinogen increased from 0.001 to 5.000 mg/mL. The values of the shift in the maximum absorbance peak ($\Delta\lambda_{max}$) for fibrinogen concentrations 0.0001, 0.01, 0.1, 1, and 10 were 4.84 ± 0.33, 8.81 ± 1.07, 13.69 ± 0.66, 20.65 ± 1.14, and 26.30 ± 1.01 nm, respectively. The $\Delta\lambda_{max}$ values for various concentrations of fibrinogen are presented in detail in Supplementary Information (Fig. S6). The $\Delta\lambda_{max}$ corresponding to the increase in the fibrinogen concentration manifested a good linear relation (R^2 = 0.99)

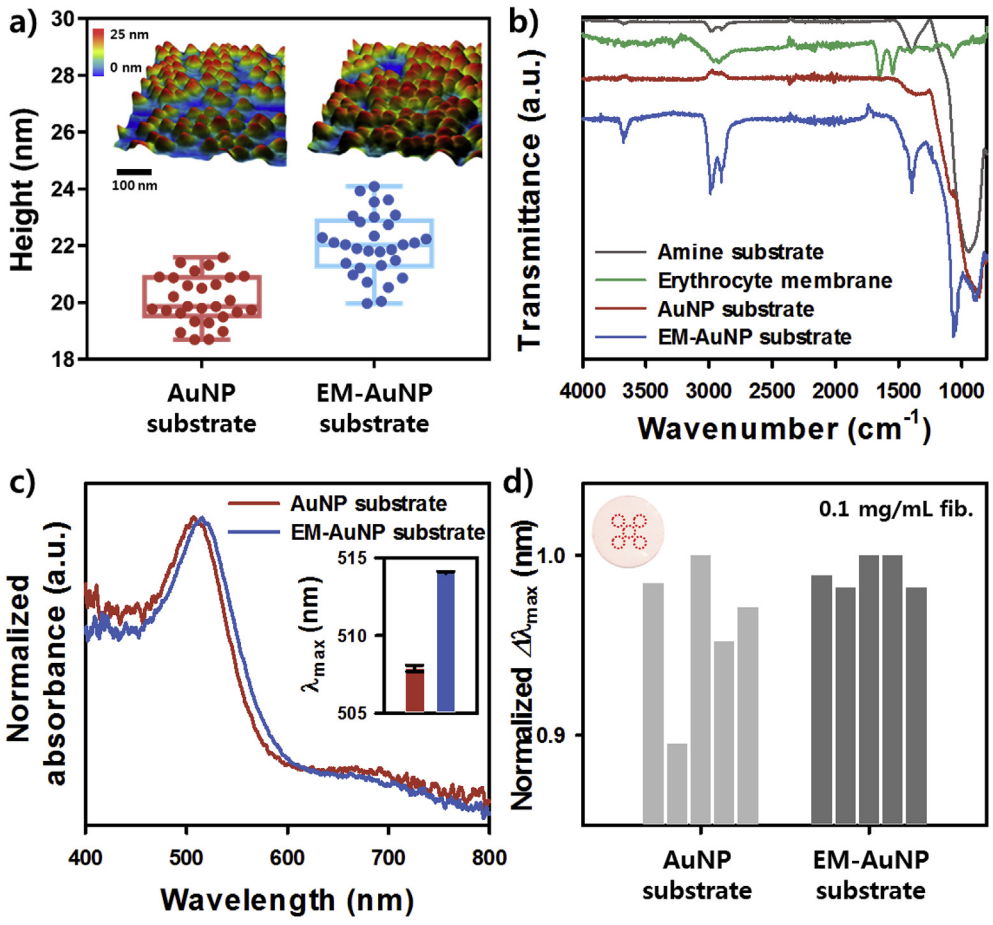

Fig. 3. Validation of blanketing of the LSPR biosensor with EMs. a) Height analysis before and after blanketing of the LSPR biosensor with EMs according to AFM topological images. b) FT-IR spectra of the amine group–functionalized substrate, substrate coated only with EMs, AuNP-based LSPR substrate, and EM-blanketed LSPR biosensor. c) LSPR spectra of the AuNP-based LSPR substrate and EM-blanketed LSPR biosensor. The inset depicts the shift in the LSPR absorbance peak (λ_{max}) of the AuNP-based LSPR substrate and EM-blanketed LSPR biosensor. d) Normalized shift of the LSPR absorbance peak ($\Delta\lambda_{max}$) in different regions on one substrate. The inset illustrates five other spots analyzed on the substrate.

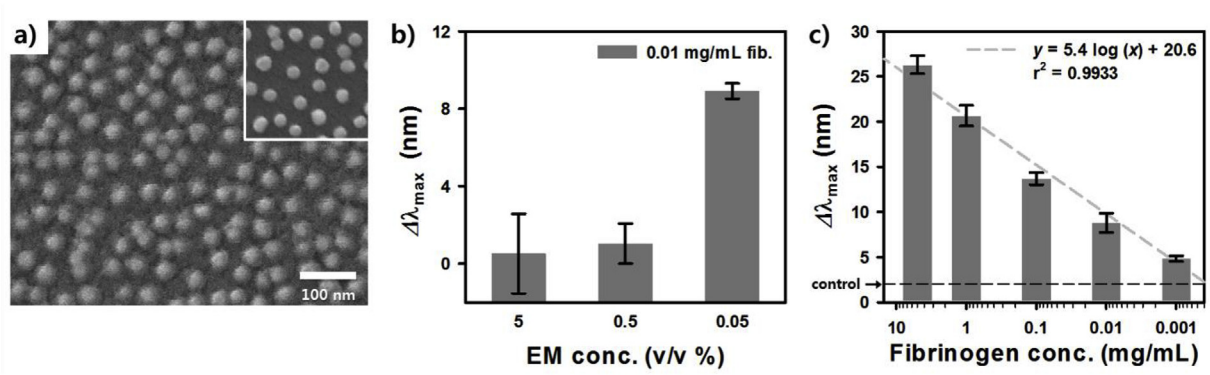

Fig. 4. Highly sensitive fibrinogen detection by the EM-blanketed LSPR biosensor. a) SEM image of the EM-blanketed LSPR biosensor treated with fibrinogen. The inset is an SEM image of the LSPR sensor before the fibrinogen treatment. b) Shift in the maximum LSPR absorbance peak depending on the concentration of EMs on the LSPR biosensor after fibrinogen treatment. c) Fibrinogen detection by the EM-blanketed LSPR biosensor over a wide range of concentrations (0.001–5.000 mg/mL).

on a logarithmic scale. The limit of detection (LOD) of this EM-blanketed LSPR biosensor for fibrinogen was 0.001 mg/mL. These results indicated that the EM blanketing could be a good way to improve fibrinogen detection sensitivity of the LSPR method.

3.5. Selectivity testing and fibrinogen detection in a plasma sample using the EM-blanketed LSPR sensor

To test specificity of the nanoplasmonic biosensor, we treated the EM-blanketed LSPR sensor with different solutions of fibrinogen (0.01 mg/mL), HSA (0.01 mg/mL), and γ-globulin (0.01 mg/mL). All the proteins were dissolved in PBS. We chose HSA and γ-globulin for the selectivity testing of the biosensor because they are the most abundant proteins in blood (Zhang et al., 2017). Fig. 5a shows relative $\Delta\lambda_{max}$ after the sensor was treated with each solution. The relative $\Delta\lambda_{max}$ % is the percentage value between the $\Delta\lambda_{max}$ of each interfering sample (*i.e.,* human serum albumin, γ-globulin, and fibrinogen) and the $\Delta\lambda_{max}$ of fibrinogen. The relative $\Delta\lambda_{max}$ % is defined as Relative $\Delta\lambda_{max}$ (%) = $\Delta\lambda_{max(interfering\ molecules)}/\Delta\lambda_{max(fibrinogen)}$, where $\Delta\lambda_{max(interfering\ molecules)}$ is the maximum wavelength change with the addition of each type of interfering molecules, and $\Delta\lambda_{max(fibrinogen)}$ is the maximum wavelength change with fibrinogen. In the case of HSA and γ-globulin, relative $\Delta\lambda_{max}$ was less than 10%, whereas the relative $\Delta\lambda_{max}$ of fibrinogen was more than 100%. Therefore, it is fair to say that

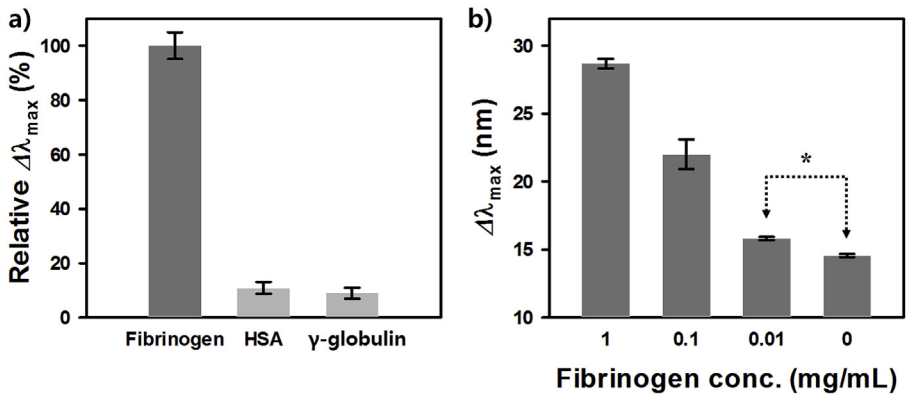

Fig. 5. Selective fibrinogen detection and quantification in blood plasma samples. a) Selectivity of the EM-blanketed biosensor in terms of LSPR detection of other proteins such as HSA and γ-globulin. b) Fibrinogen detection over a wide range of concentrations (0.001–1.000 mg/mL) in a 10-fold–diluted plasma sample. The LOD was 0.01 mg/mL (*p-value* < 0.0001).

fibrinogen is selectively detected by EM-blanketed LSPR biosensors as compared to other proteins such as HSA and γ-globulin.

We conducted further experiments to verify whether the LSPR biosensor can detect fibrinogen in human plasma samples. We validated the level of fibrinogen in the plasma by ELISA method. (Fig. S7). Fig. 5b illustrates the changes in $\Delta\lambda_{max}$ of the EM-blanketed LSPR biosensor after treatment with a 10-fold–diluted plasma sample spiked with 0–1 mg/mL fibrinogen. The values of shift of the $\Delta\lambda_{max}$ for fibrinogen concentrations 0, 0.01, 0.1, and 1 were 14.56 ± 0.10, 15.81 ± 0.12, 22.02 ± 1.09, and 28.69 ± 0.35 nm, respectively. We found that fibrinogen detection was possible in a range of 0.01–1 mg/mL. Compared to the results obtained in PBS, the sensitivity of fibrinogen detection was somewhat worse due to unknown proteins present in the plasma sample. The LOD of this sensor for fibrinogen was found to be 0.01 mg/mL (*p*-value < 0.0001) in the plasma sample. Judging by these results, we believe that this selective LSPR sensor has a great potential for detecting fibrinogen in actual samples.

4. Conclusions

In this work, we devised a highly sensitive EM-blanketed LSPR biosensor that can detect fibrinogen over a wide range of concentrations, even in human blood plasma samples. In our experiments, it was demonstrated that the concentrations of fibrinogen could be differentiated in the range of 0.001–5.000 mg/mL after coating of the surface of the LSPR biosensor with EMs. This wide-range fibrinogen assay has excellent advantages in detecting a fibrinogen excess or deficiency in plasma samples. The strategy of coating the substrate with EMs is advantageous for the detection of fibrinogen using the nanoplasmonic phenomenon; an appropriate concentration of EMs can enable stable attachment and retention of AuNPs on the substrate. This approach can not only improve the LSPR signal but also measure a wide range of fibrinogen concentrations. Additionally, it is possible to increase the efficiency of capture of fibrinogen by evenly spreading the receptor present on the EMs across the substrate, thus obviating additional labeling. This strategy can both improve the sensitivity of fibrinogen detection and offer a selective fibrinogen assay unaffected by other proteins. As a pilot study, we believe that this new method involving EMs holds great promise for fibrinogen sensing for the prevention of various diseases.

CRediT authorship contribution statement

Seongjae Jo: Conceptualization, Validation, Investigation, Formal analysis. **Insu Kim:** Conceptualization, Resources. **Wonseok Lee:** Writing - original draft. **Minwoo Kim:** Visualization, Investigation. **Joohyung Park:** Investigation, Formal analysis. **Gyudo Lee:** Supervision. **Dae Sung Yoon:** Supervision. **Jinsung Park:** Writing - review & editing.

Acknowledgements

This work was supported by a National Research Foundation of Korea grant, funded by the South Korean government (NRF-2017M3A9F1031229, NRF-2017R1E1A1A01075439, and NRF-2018M3C1B7020722).

Appendix A. Supplementary data

Supplementary data to this article can be found online at https://doi.org/10.1016/j.bios.2019.04.030.

Declaration of interests

The authors declare that they have no competing interests.

References

Atar, N., Eren, T., Yola, M.L., 2015a. A molecular imprinted SPR biosensor for sensitive determination of citrinin in red yeast rice. Food Chem. 184, 7–11.
Atar, N., Eren, T., Yola, M.L., Wang, S., 2015b. A sensitive molecular imprinted surface plasmon resonance nanosensor for selective determination of trace triclosan in wastewater. Sensor. Actuator. B Chem. 216, 638–644.
Bach, T.L., Barsigian, C., Chalupowicz, D.G., Busler, D., Yaen, C.H., Grant, D.S., Martinez, J., 1998. VE-cadherin mediates endothelial cell capillary tube formation in fibrin and collagen Gels1. Exp. Cell Res. 238 (2), 324–334.
Bastús, N.G., Comenge, J., Puntes, V., 2011. Kinetically controlled seeded growth synthesis of citrate-stabilized gold nanoparticles of up to 200 nm: size focusing versus ostwald ripening. Langmuir 27 (17), 11098–11105.
Brittin, G.M., Rafinia, H., Raval, D., Werner, M., Brown, D., 1972. Evaluation of single radial immunodiffusion for quantitation of plasma fibrinogen. Am. J. Clin. Pathol. 57 (1), 89–94.
Campuzano, S., Salema, V., Moreno-Guzmán, M., Gamella, M., Yáñez-Sedeño, P., Fernández, L.A., Pingarrón, J.M., 2014. Disposable amperometric magnetoimmunosensors using nanobodies as biorecognition element. Determination of fibrinogen in plasma. Biosens. Bioelectron. 52, 255–260.
Carvalho, F.A., Connell, S., Miltenberger-Miltenyi, G., Pereira, S.V., Tavares, A., Ariëns, R.A.S., Santos, N.C., 2010. Atomic force microscopy-based molecular recognition of a fibrinogen receptor on human erythrocytes. ACS Nano 4 (8), 4609–4620.
Carvalho, F.A., de Oliveira, S., Freitas, T., Gonçalves, S., Santos, N.C., 2011. Variations on fibrinogen-erythrocyte interactions during cell aging. PLoS One 6 (3), e18167.
Chen, Y.-Y., Tseng, C.-W., Chang, H.-Y., Hung, Y.-L., Huang, C.-C., 2011. Gold nanoparticle-based colorimetric assays for coagulation-related proteins and their inhibition reactions. Biosens. Bioelectron. 26 (7), 3160–3166.
Dejana, E., Lampugnani, M.G., Giorgi, M., Gaboli, M., Marchisio, P.C., 1990. Fibrinogen induces endothelial cell adhesion and spreading via the release of endogenous matrix proteins and the recruitment of more than one integrin receptor. Blood 75 (7), 1509.

Deng, Z.J., Liang, M., Toth, I., Monteiro, M.J., Minchin, R.F., 2012. Molecular interaction of poly(acrylic acid) gold nanoparticles with human fibrinogen. ACS Nano 6 (10), 8962–8969.
Ernst, E., 1993. The role of fibrinogen as a cardiovascular risk factor. Atherosclerosis 100 (1), 1–12.
Feuz, L., Jönsson, P., Jonsson, M.P., Höök, F., 2010. Improving the limit of detection of nanoscale sensors by directed binding to high-sensitivity areas. ACS Nano 4 (4), 2167–2177.
Garvey, M.B., Black, J.M., 1972. The detection of fibrinogen/fibrin degradation products by means of a new antibody-coated latex particle. J. Clin. Pathol. 25 (8), 680.
Grimaldi, I.A., Testa, G., Persichetti, G., Loffredo, F., Villani, F., Bernini, R., 2016. Plasma functionalization procedure for antibody immobilization for SU-8 based sensor. Biosens. Bioelectron. 86, 827–833.
Guedes, A.F., Carvalho, F., Lousada, N., Sargento, L., Santos, N.C., 2017. Atomic force microscopy as a tool to evaluate the risk of cardiovascular diseases in patients. Biophys. J. 112 (3, Suppl. 1) 303a.
Hong, Y., Jo, S., Park, J., Park, J., Yang, J., 2018. High sensitive detection of copper II ions using D-penicillamine-coated gold nanorods based on localized surface plasmon resonance. Nanotechnology 29 (21), 215501.
Kaptoge, S., Angelantonio, E.D., Pennells, L, Wood, Angela M., 2012. C-reactive protein, fibrinogen, and cardiovascular disease prediction. N. Engl. J. Med. 367 (14), 1310–1320.
Kim, I., Kwon, D., Lee, D., Lee, T.H., Lee, J.H., Lee, G., Yoon, D.S., 2018. A highly permselective electrochemical glucose sensor using red blood cell membrane. Biosens. Bioelectron. 102, 617–623.
Kozicki, M., Creek, D.J., Sexton, A., Morahan, B.J., Wesełucha-Birczyńska, A., Wood, B.R., 2015. An attenuated total reflection (ATR) and Raman spectroscopic investigation into the effects of chloroquine on Plasmodium falciparum-infected red blood cells. Analyst 140 (7), 2236–2246.
Laurens, N., Koolwijk, P., De Maat, M.P.M., 2006. Fibrin structure and wound healing. J. Thromb. Haemost. 4 (5), 932–939.
Lee, J.H., Ryu, K.W., Kim, S.J., Bae, J.-M., 2004. Preoperative plasma fibrinogen levels in gastric cancer patients correlate with extent of tumor. Hepato-Gastroenterology 51, 1860–1863.
Levy, J.H., Welsby, I., Goodnough, L.T., 2013. Fibrinogen as a therapeutic target for bleeding: a review of critical levels and replacement therapy. Transfusion 54 (5), 1389–1405.
Lowe, G.D.O., Rumley, A., Mackie, I.J., 2004. Plasma fibrinogen. Ann. Clin. Biochem. 41 (6), 430–440.
Mackie, I.J., Kitchen, S., Machin, S.J., Lowe, G.D.O., 2003. Guidelines on fibrinogen assays. Br. J. Haematol. 121 (3), 396–404.
Miesbach, W., Schenk, J., Alesci, S., Lindhoff-Last, E., 2010. Comparison of the fibrinogen Clauss assay and the fibrinogen PT derived method in patients with dysfibrinogenemia. Thromb. Res. 126 (6), e428–e433.
Neerman-Arbez, M., Casini, A., 2018. Clinical consequences and molecular bases of low fibrinogen levels. Int. J. Mol. Sci. 19 (1), 192.
Özkan, A., Atar, N., Yola, M.L., 2019. Enhanced surface plasmon resonance (SPR) signals based on immobilization of core-shell nanoparticles incorporated boron nitride nanosheets: development of molecularly imprinted SPR nanosensor for anticancer drug, etoposide. Biosens. Bioelectron. 130, 293–298.
Palumbo, J.S., Kombrinck, K.W., Drew, A.F., Grimes, T.S., Kiser, J.H., Degen, J.L., Bugge, T.H., 2000. Fibrinogen is an important determinant of the metastatic potential of circulating tumor cells. Blood 96 (10), 3302.
Piccione, G., Casella, S., Giannetto, C., Giudice, E., 2010. Effect of storage conditions on prothrombin time, activated partial thromboplastin time and fibrinogen concentration on canine plasma samples. J. Vet. Sci. 11 (2), 121–124.
Polterauer, S., Grimm, C., Seebacher, V., Concin, N., Marth, C., Tomovski, C., Husslein, H., Leipold, H., Hefler-Frischmuth, K., Tempfer, C., Reinthaller, A., Hefler, L., 2009. Plasma fibrinogen levels and prognosis in patients with ovarian cancer: a multicenter study. Oncol. 14 (10), 979–985.
Sahni, A., Sporn, L.A., Francis, C.W., 1999. Potentiation of endothelial cell proliferation by fibrin(ogen)-bound fibroblast growth factor-2. J. Biol. Chem. 274 (21), 14936–14941.
Schifreen, R.S., Cembrowski, G.S., Campbell, D.C., Craig, A.R., Demyanovich, N.D., Jurga-Hall, P.A., Reider, M.C., Schwartz, M.W., Tuhy, P.M., Waller, S.J., 1985. A quantitative automated immunoassay for fibrinogen/fibrin degradation products. Clin. Chem. 31 (9), 1468.
Shiose, S., Hata, Y., Noda, Y., Sassa, Y., Takeda, A., Yoshikawa, H., Fujisawa, K., Kubota, T., Ishibashi, T., 2004. Fibrinogen stimulates in vitro angiogenesis by choroidal endothelial cells via autocrine VEGF. Graefes Arch. Clin. Exp. Ophthalmol. 242 (9), 777–783.
Simpson-Haidaris, P.J., Rybarczyk, B., 2001. Tumors and fibrinogen. Ann. N. Y. Acad. Sci. 936 (1), 406–425.
Tennent, G.A., Brennan, S.O., Stangou, A.J., O'Grady, J., Hawkins, P.N., Pepys, M.B., 2007. Human plasma fibrinogen is synthesized in the liver. Blood 109 (5), 1971.
Wu, Q., Sheehan, J.P., Tsiang, M., Lentz, S.R., Birktoft, J.J., Sadler, J.E., 1991. Single amino acid substitutions dissociate fibrinogen-clotting and thrombomodulin-binding activities of human thrombin. Proc. Natl. Acad. Sci. U. S. A. 88 (15), 6775.
Yola, M.L., Atar, N., Erdem, A., 2015. Oxytocin imprinted polymer based surface plasmon resonance sensor and its application to milk sample. Sensor. Actuator. B Chem. 221, 842–848.
Yola, M.L., Atar, N., Eren, T., 2014a. Determination of amikacin in human plasma by molecular imprinted SPR nanosensor. Sensor. Actuator. B Chem. 198, 70–76.
Yola, M.L., Eren, T., Atar, N., 2014b. Molecular imprinted nanosensor based on surface plasmon resonance: application to the sensitive determination of amoxicillin. Sensor. Actuator. B Chem. 195, 28–35.
Zhang, X., Zhang, J., Zhang, F., Yu, S., 2017. Probing the binding affinity of plasma proteins adsorbed on Au nanoparticles. Nanoscale 9 (14), 4787–4792.